CIRP Annals - Manufacturing Technology 71 (2022) 101–104

Contents lists available at ScienceDirect

CIRP Annals - Manufacturing Technology

journal homepage: https://www.editorialmanager.com/CIRP/default.aspx

Effect of crystallography on residual stresses during ultra-precision machining of sapphire

Aditya Nagaraj, Sangkee Min (2)*

Department of Mechanical Engineering, University of Wisconsin-Madison, WI 53706, USA

ARTICLE INFO

Article history:
Available online 26 April 2022

Keywords:
Residual stress
Anisotropy
Sapphire

ABSTRACT

Residual stresses play an important role in determining the quality of a machined surface during ultra-precision machining (UPM) of ceramics by initiating cracks at premature loads. In this study, the anisotropy in residual stresses resulting from UPM of two crystallographic planes of sapphire is investigated using micro-Raman spectroscopy. An analytical model is then used to improve our understanding of plastic deformation during UPM and its contribution to residual stress. Results show a strong dependence of residual stress magnitude on the slip and fracture systems activated during machining which are anisotropic based on the cutting direction.

1. Introduction

In many applications where single crystal ceramics are used, such as optics and electronics, residual stresses can hinder the functionality of the manufactured component. However, almost all manufacturing processes, including grinding and UPM leave behind residual stresses due to plastic deformation caused in the workpiece. Further, most machining operations require multiple passes over the same region of the workpiece and residual stresses can build up over time and lead to brittle fractures, which can be detrimental to the application of the ceramic [1,2]. Thus, it is of utmost importance to understand the mechanisms leading to the formation of residual stress and to develop methods to control its magnitude.

The amount of residual stresses have been quantified using various techniques such as angle polishing, Raman spectroscopy, and X-ray diffraction. Using Raman spectroscopy, researchers observed that residual stresses gradually change from tensile to compressive state as the scratch depth was increased during ultrasonic vibration assisted and laser assisted machining of sapphire [3,4]. Yan et al. studied the effect of crystallographic orientation on subsurface damage evolution in single crystal silicon using micro-Raman spectroscopy and XTEM and correlated the subsurface damage amount to deformation in the material using the slip factor [5].

Lin et al. studied the effect of process parameters on residual stresses during ultra-precision machining of NiP alloy using FEM simulation and reported increasing compressive residual stresses with increasing cutting velocity. The compressive residual stresses increased as the depth of cut was increased, up to a certain threshold value and then began to decrease [6].

Yoon et al. investigated the effect of two-step machining on critical depth of cut for various crystallographic orientations on C-plane of sapphire and found that damage from the first cut reduces the critical depth of cut during subsequent machining over the same area [7].

The research so far has mostly provided quantitative estimates of residual stresses and different causes such as plastic deformation, phase transformation and temperature gradients. However, study on the anisotropic nature of residual stresses and estimates based on the analysis of plastic deformation tendencies of different cutting directions have not been investigated in detail. The present research looks at the anisotropy in residual stresses through UPM experiments on sapphire and micro-Raman spectroscopy. The resulting residual stress magnitudes are explained by predicting the amount of plastically deformed material remaining in a machined workpiece.

2. Prediction of plastic deformation using an analytical model

The major cause of residual stresses in machined ceramics is plastic deformation. During UPM of ceramics, material removal can be classified into two categories – ductile and brittle. Although severe plastic deformation occurs during machining, a large portion of the plastically deformed material is removed either in the form of chips or through brittle fracture. However, due to the anisotropic nature of single crystal ceramics, the mechanisms by which plastic deformation occurs depends on many process parameters such as cutting direction, depth of cut, feed rate, etc. Based on force measurements during machining, the likelihood of activation of different slip systems that initiate plastic deformation can be calculated using Eq. (1) [8].

$$P'_i = m'_i/(\tau_i^{crit}/\min_i \tau_i^{crit}) \quad (1)$$

Where P_i' is defined as the plastic deformation parameter which represents the likelihood of activation of the *i*th slip or twinning system, m_i' is the modified Schmid factor that considers the angle the resultant force makes with a given slip system and τ_i^{crit} is the critical resolved shear stress of the *i*th slip or twinning system. Based on the

* Corresponding author.
E-mail address: sangkee.min@wisc.edu (S. Min).

https://doi.org/10.1016/j.cirp.2022.04.004
0007-8506/

likelihood of activation of a particular slip/twinning system for a given cutting direction, the angle the slip system makes with the workpiece surface is then calculated. For those slip/twinning systems that make shallow angles with the workpiece surface, the region of plastically deformed material is generally close to the surface and is removed during chip formation at low depths of cut or by fracture beyond the critical depth of cut (CDC) where ductile to brittle transition (DBT) occurs. This situation is hypothesised to have a small value of residual stresses. On the contrary, if the most likely slip system forms a steep angle with the workpiece surface, not all the plastically deformed material would be removed by the chip or fracture, leading to a higher magnitude of residual stress. In some cutting directions, when multiple slip/twinning systems have similar or low probability of activation, there is chance of dislocation entanglement due to activation of multiple slips and once again the plastic deformation does not extend to deeper regions in the subsurface. A schematic of this hypothesis is shown in Fig. 1.

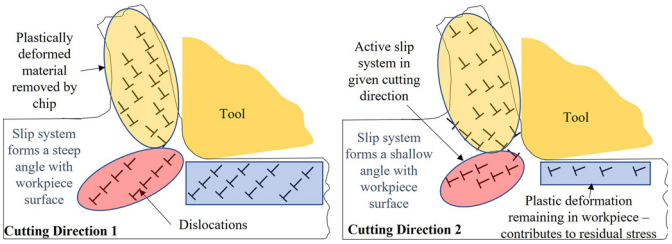

Fig. 1. Schematic showing initiation and evolution of two different slip systems during UPM of sapphire.

3. Experiment details

3.1. Ultra-precision machining

Ultra-precision machining experiments were carried out on C- and R- oriented sapphire substrates (both sides polished) having dimensions of 10 mm × 10 mm × 0.5 mm (produced by Czochralski technique, M.T.I Corp., U.S.A) on a 5-axis ultra-precision machine tool (ROBONANO α–0*i*B, FANUC Corporation, Japan) having 1 nm command resolution in the linear axis and 1 micro degree command resolution in the rotary axis. Plunge cuts of increasing depth (0–500 nm) were performed in different cutting directions 30° apart using a PCD tool with 0.5 mm nose radius (grade: BL-PCD, A.L.M.T. Corp., Japan) at 5 mm/min. Cutting forces used for analytical calculations were measured using a dynamometer (Kistler Corp., Switzerland). The setup is shown in Fig. 2. Since the deformation characteristics of C- and R-planes of sapphire showed two-fold mirror symmetry, machining and analysis was performed for only half of the directions [9]. In the case of C- and R-planes, the cutting directions investigated were oriented with $[11\bar{2}0]$ as 0°, $[1\bar{1}00]$ as 90° in the case of C-plane and $[\bar{1}\bar{1}20]$ as 180° for R-plane. Additional details regarding the setup and CDC distribution can be found in [8,9].

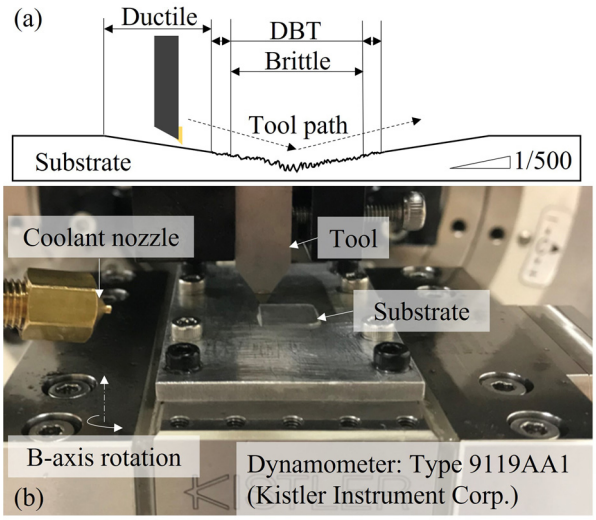

Fig. 2. (a)Schematic of plunge cutting; (b) Machining setup.

3.2. Residual stress measurements using Raman spectroscopy

Residual stress measurements were carried out on a micro-Raman spectrometer (LabRAM HR Evolution, Horiba Ltd., Japan) using a 633 nm laser, 100× objective (0.9 NA), 100 μm confocal hole and 1800 mm^{-1} grating. For the analysis, 418 cm^{-1} peak was chosen as it has the highest signal intensity. The measurements were carried out in the ductile, ductile-brittle transition and brittle regions of the machined cuts with the cutting direction oriented vertically in the field of view (Fig. 6). The peak position in the machined area was determined by taking an average value from 24 points in the center of the cut in each region. 2 measurements (10 s each) were taken at each point to eliminate cosmic ray spikes. The 24 points were arranged in a 6 × 4 grid, ~ 12 µm wide and 9 µm high. The nature of residual stresses was determined by comparing the peak position in the machined area with the peak position from a region free of machining. A peak shift to lower wavenumbers indicates tensile residual stress whereas a peak shift to higher wavenumbers indicates compressive residual stresses. The residual stress magnitude presented is an equivalent magnitude determined through data extrapolated from a diamond anvil test resulting in a correlation of 2.2 cm^{-1}/GPa peak shift [10]. The exact magnitude of residual stress is dependent on the stress field generated during machining but, due to challenges associated with determining the exact nature of the stress field, this has been reserved for future work.

4. Results and discussion

4.1. Residual stress measurements

The magnitude of equivalent residual stress on R-plane of sapphire is shown in Fig. 3. With regard to the reference region, free of machining, the residual stresses were tensile in nature for all the cases except in the brittle region for 90° cutting. More importantly, the residual stress magnitude strongly depends on the cutting direction. The magnitude of residual stresses varies from tens of MPa up to 150 MPa in the case of 150° cutting direction. In most cases, as the depth of cut is increased, the residual stress magnitude decreases due to stress relieved by crack initiation. However, in the case of 180° cutting direction, the magnitude of residual stresses is maximum in the brittle region. The reason for this is because the cracks in this cutting direction are very sparse and the CDC is large [8,9]. As a result, the residual stresses keep accumulating as the depth of cut is increased and are relieved only in localized regions beyond the CDC. Hence it is important to consider both the plastic deformation amount as well as crack morphology while estimating residual stresses.

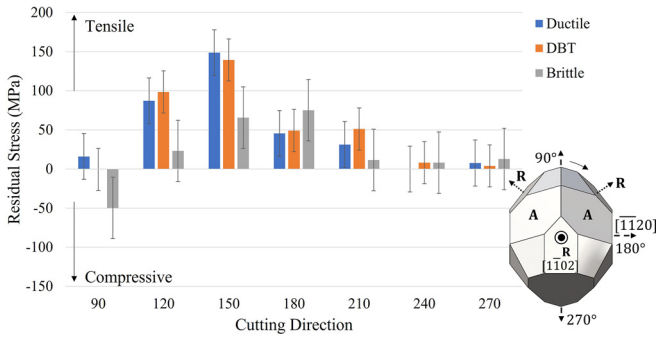

Fig. 3. Residual stresses per cutting direction on R-plane of sapphire.

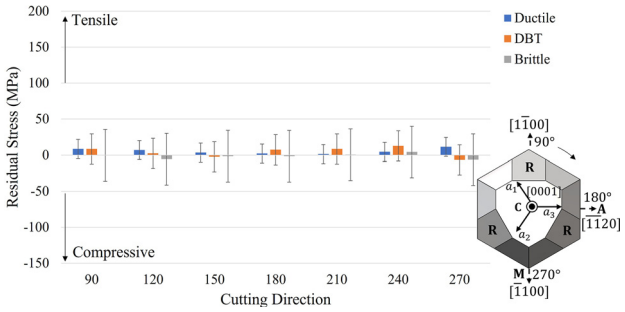

Fig. 4. Residual stresses per cutting direction on C-plane of sapphire.

The magnitude of equivalent residual stress on C-plane of sapphire is shown in Fig. 4. Unlike the case of R-plane, the magnitude of residual stresses on C-plane is almost negligible and uniformly so across multiple cutting directions.

4.2. Analysis of deformation mode and correlation to residual stresses

The variation in plastic deformation parameter with cutting direction for the three depths of cut corresponding to the Raman measurements on R-plane are shown in Fig. 5(a). The angle made by the dominant plastic deformation mechanisms with the machined surface is shown in Fig. 5(b). In the ductile and DBT regions, rhombohedral twinning on an adjacent R-plane (R2 TW) is the dominant mechanism for 150°, 180° and, 210° cutting directions which explains the large value of residual stress magnitude. In the case of 210°, the second dominant mechanism is rhombohedral twinning on the same R-plane as the cutting (R1 TW) which might lead to dislocation entanglement and hence reducing the amount of plastic deformation deeper into the workpiece and consequently the residual stress. In the case of 240° and 270° cutting direction, rhombohedral twinning on the same plane as the cutting is dominant which results in deformation parallel to the surface and at a shallow depth which is removed by chip formation. In the case of 90° cutting direction, although the dominant mechanism is basal twinning, the CDC for this cutting direction is the smallest. Hence, not much residual stress is thought to accumulate in the ductile regions. In the case of 120° cutting direction, the dominant plastic deformation is basal slip which forms an angle of 47° with the machined surface resulting in plastic deformation that extends deeper into the subsurface.

Looking at the brittle regions of the different cutting directions (Fig. 5(c)), the fractures in the case of 180° and 150° cutting directions were sparse with large regions of ductile machining in between cracks. As a result, a decrease in residual stress magnitude from DBT to brittle region was not observed in 180° case and a small amount was observed for 150°. In the case of 120°, 210° and 240° cutting directions, prismatic and rhombohedral fractures covered the brittle region and were deep. This explains the sharp reduction in residual stress magnitude in these directions. In the case of 270° cutting direction, shallow prismatic fractures were observed. As the residual stress magnitude in this direction was already small, not much change was observed. In the case of 90° cutting direction, basal and prismatic fractures were observed in a banded fashion likely caused by alternative pile up of material through plastic deformation and fractures relieving the stresses partially. The pile-up is the likely reason for compressive residual stresses in this direction.

The variation in plastic deformation parameter with cutting direction for the three depths of cut corresponding to the Raman measurements on C-plane are shown in Fig. 5(d). Unlike the R-plane, there is not much anisotropy in the dominant plastic deformation mechanisms. In the case of 120°, 150°, 240° and 270° cutting directions, the dominant mechanism across depths of cut is basal slip or basal twinning which causes deformation parallel to the workpiece surface (0° in Fig. 5(e)) and forms a shallow layer of plastic deformation that is easily removed by chip formation or fracture at larger depths of cut. Considering the 180° cutting direction, basal slip is the dominant mechanism at low depths of cut but changes to rhombohedral

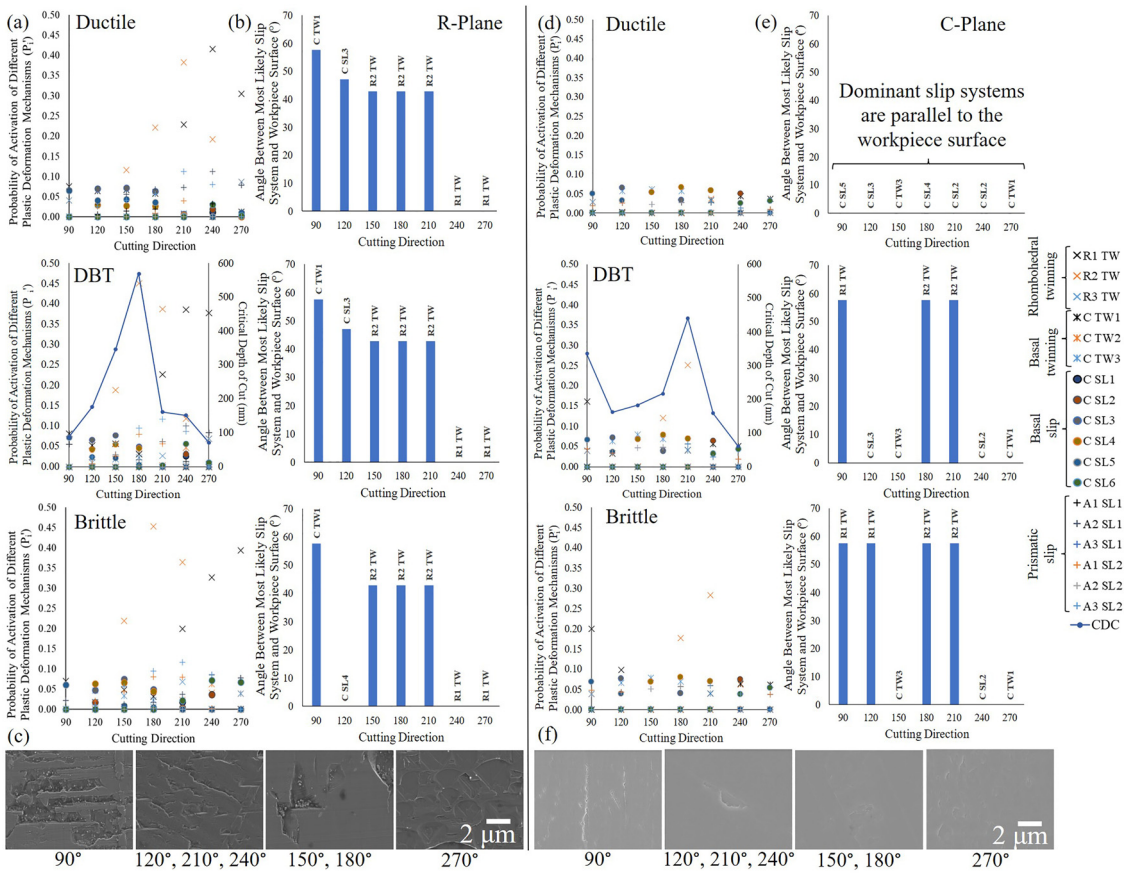

Fig. 5. Analysis of plastic deformation parameter and crack morphology on R- and C- planes of sapphire.

twinning as the depth of cut is increased. However, the probabilities of activation of all the mechanisms remain low and there could be dislocation entanglement leading to lower depth of plastic deformation. The case of 90° and 210° is similar to that of 180° with a slight difference being rhombohedral twinning is the dominant mechanism even at low depths. However, low values of residual stress magnitude are likely due to dislocation entanglement resulting in a shallow plastic deformation region.

Considering the fracture mechanisms on the C-plane (Fig. 5(f)), prismatic fractures dominate across different cutting directions. Unlike the R-plane, cracks are not highly concentrated, as seen in certain directions (270° of the R-plane). These shallow and spaced-out fractures thus relieve the small magnitude of residual stresses and do not cause much of a change to the residual stress state.

5. Optimized 2-step cutting strategy

Since machining operations in general require multiple passes over the same regions of the workpiece to get from raw material to finished product, it is important to understand the effect of residual stresses during multi-pass cutting operations. The aim of this section was to test a 2-step machining strategy that improves the machining throughput while producing a ductile surface with minimal residual stresses. This test experiment was conducted on the R-plane of sapphire since there is a clear trend of anisotropy in residual stress magnitude. For the machining strategy, first, a machined area (1 mm × 0.6 mm) was created by cutting in the 270° cutting direction at a constant depth of 300 nm (~3 x CDC) and pitch of 15 µm. The subsequent machined area was created by cutting in the 180° cutting direction over the previously machined region. For the subsequent machining, plunge cuts with a maximum depth of cut of 400 nm (~0.7 x CDC) and pitch of 15 µm were used. 270° was chosen for the first cut due to the low residual stress magnitude in the brittle region and high concentration of cracks would likely cause local regions of compressive stresses [11]. 180° was chosen for the subsequent cut due to the high value of CDC which would aid in removing cracks on the surface and low value of residual stresses in the ductile region. Optical microscope images of the machined areas are shown in Fig. 6. Residual stress measurements were performed using the same parameters described in Section 3. The magnitude of residual stress was estimated by comparing the peak position in the polished region, primary machining region (270° cutting) and subsequent machined region (180° cutting) by considering the average peak position from 72 points in a ~36 µm × 12 µm area.

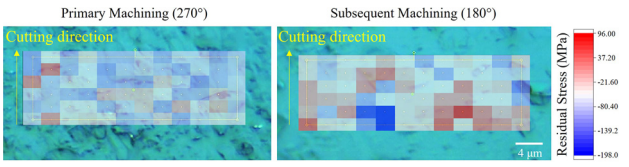

Fig. 6. Residual stress measurement on machined surface.

In terms of the residual stress measurements, compared to the polished region, the region machined in the 270° cutting direction had an equivalent residual stress value of ~ −70 MPa (compressive). Although the value is closer to 0 MPa in the case of the single cut, the high density of cracks in the machined area may contribute to the compressive stresses [11]. The subsequent machined area in the 180° cutting direction had an equivalent residual stress value of ~ −40 MPa (compressive) with respect to the polished region. This reduction in compressive magnitude of stress is likely due to ductile machining and removal of surface cracks by the subsequent machining.

Evaluating the surface of the subsequent machined region, the cracks from primary cutting are partially removed. Further optimization of the depths of cuts of the primary and subsequent cutting would be necessary to remove most of the cracks from the surface.

6. Conclusion

The anisotropy in residual stresses on ultra-precision machined C- and R-planes of sapphire was quantified using micro-Raman spectroscopy and the nature of residual stresses were tensile in nature for most of the cutting directions. The measurements showed minimal residual stresses on C-plane due to plastic deformation being concentrated close to the surface layers which were subsequently removed by chip formation or fracture. Whereas, in the case of R-plane, tensile residual stresses up to 150 MPa were measured and plastic deformation mechanisms extending deeper into the subsurface are predicted based on analytical calculations which result in higher levels of residual stresses. A two-step machining strategy was also evaluated where surface crack removal was demonstrated at the same time imparting a slightly compressive residual stress state which would be beneficial to machined ceramics.

In future work, mechanisms of subsurface damage will be investigated, and this approach will be extended to other ceramic materials. Based on the results, other machining strategies that improve machining throughput while minimizing residual stresses and subsurface damage will be developed.

Declaration of Competing Interest

The authors declare that they have no known competing financial interests or personal relationships that could have appeared to influence the work reported in this paper.

Acknowledgments

This material is based on work supported in part by the National Science Foundation under the award number CMMI-2008563. The authors gratefully acknowledge use of facilities and instrumentation at the UW-Madison Wisconsin Centers for Nanoscale Technology partially supported by the NSF through the University of Wisconsin Materials Research Science and Engineering Center (DMR-1720415). The authors would also like to thank FANUC Corporation, Japan for the donation of the 5-axis ultra-precision machine tool, ROBONANO $\alpha-0iB$ and A.L.M.T Corporation, Japan for providing the discounted diamond tools used in this study. The authors would like to thank Suk Bum Kwon for his assistance in performing the experiments and analysis.

References

[1] Samuel R, Chandrasekar S, Farris TN, Licht RH (1989) Effect of Residual Stresses on the Fracture of Ground Ceramics. *Journal of the American Ceramic Society* 72 (10):1960–1966.
[2] Khan ZA, Hadfield M, Tobe S, Wang Y (2005) Ceramic Rolling Elements with Ring Crack Defects—A Residual Stress Approach. *Materials Science and Engineering: A* 404(1–2):221–226.
[3] Zhang C, Feng P, Zhang J (2013) Ultrasonic Vibration-Assisted Scratch-Induced Characteristics of C-Plane Sapphire with a Spherical Indenter. *International Journal of Machine Tools and Manufacture* 64:38–48.
[4] Langan SM, Ravindra D, Mann AB (2019) Mitigation of Damage During Surface Finishing of Sapphire Using Laser-Assisted Machining. *Precision Engineering* 1 (56):1–7.
[5] Yan J, Asami T, Harada H, Kuriyagawa T (2012) Crystallographic Effect on Subsurface Damage Formation in Silicon Microcutting. *Annals of the CIRP* 61(1):131–134.
[6] Lin ZC, Lai WL, Lin HY, Liu CR (2000) The Study of Ultra-Precision Machining and Residual Stress for NiP Alloy with Different Cutting Speeds and Depth of Cut. *Journal of Materials Processing Technology* 97(1–3):200–210.
[7] Yoon HS, Kwon SB, Nagaraj A, Min S (2020) Effect of the Initial-Flaw on Crack-Propagation in Two-Step Cutting of Monocrystalline Sapphire. *Journal of Manufacturing Processes* 56:1211–1218.
[8] Kwon SB, Nagaraj A, Yoon HS, Min S (2020) Study of Material Removal Behavior on R- Plane of Sapphire During Ultra-Precision Machining Based on Modified Slip-Fracture Model. *Nanotechnology and Precision Engineering* 3(3):141–155.
[9] Yoon HS, Kwon SB, Nagaraj A, Lee S, Min S (2018) Study of Stress Intensity Factor on the Anisotropic Machining Behavior of Single Crystal Sapphire. *Annals of the CIRP* 67(1):125–128.
[10] Gallas MR, Chu YC, Piermarini GJ (1995) Calibration of the Raman Effect in $\alpha-Al_2O_3$ Ceramic for Residual Stress Measurements. *Journal of Materials Research* 10(11):2817–2822.
[11] Wei SL, et al. (2017) Investigation on Surface Residual Stress Distribution and Evaluation of Engineering Ceramics in Rotary Ultrasonic Grinding Machining. *Proceedings of the Institution of Mechanical Engineers Part C: Journal of Mechanical Engineering Science* 231(15):2773–2782.